Lipophilicity prediction of three photosensitizers by liquid–liquid extraction, HPLC, and DFT methods

Bauyrzhan Myrzakhmetov, Jonathan Honorien, Philippe Arnoux, René Fournet, Irina Tsoy, Céline Frochot, René Fournet

Lipophilicity prediction of 3 photosensitizers by liquid-liquid extraction, HPLC, and DFT methods

Bauyrzhan Myrzakhmetov[1, 2], Jonathan Honorien[1], Philippe Arnoux[1], René Fournet[1], Irina Tsoy[2] and Céline Frochot[1, *]

[1]LRGP UMR 7274, CNRS, University of Lorraine, Nancy, France.
[2]Department of Chemistry and Chemical Technology, M.Kh. Dulaty Taraz Regional University, Taraz 080012, Kazakhstan.

*Corresponding author e-mail: celine.frochot@univ-lorraine.fr (Celine Frochot)

ABSTRACT

Photodynamic therapy (PDT) is a method of treating precancerous diseases and malignant neoplasms. The efficacy of PDT depends on different parameters such as light dosimetry, oxygen availability, and photophysical and physical-chemical properties of the photosensitizer. In PDT, a photosensitizer is activated using light to promote oxygen photosensitization and cellular transport plays a key role in the reach of it the desired tissue. In particular, to know the effectiveness of the drug delivery in PDT and its dosage forms to target damaged organs, along with such characteristics as water solubility, it is important to know the ability of a substance to penetrate through cell membrane or accumulate in it. The lipophilicity is used to quantify the above-described abilities. We evaluated the lipophilicity of three selected PS protoporphyrin IX, pyropheophorbide-a and photofrin by means of three different methods: octanol-water distribution methods (Shake-flask), reversed-phase high-performance liquid chromatography (HPLC) and theoretical calculations based on density functional theory (DFT). We describe and compare the results of these various methods.

1 | INTRODUCTION

Photodynamic therapy (PDT) requires three elements that are light, oxygen and a photoactivable molecule called the photosensitizer. Under light illumination, the photosensitizer (PS) is excited and, in the presence of oxygen, induces the formation of singlet oxygen or other reactive oxygen species that destroy the surrounding species [1]. PDT can be used to kill cancer cells, fungi, bacteria, and viruses. If light dosimetry should be carefully controlled, the choice of the PS is another important factor in inducing an adequate photodynamic effect. A PS should ideally possess an absorption peak in the near-infrared region that allows enough light penetration into tissues. Moreover, it should be preferentially retained in the diseased tissues compared to healthy ones and fast eliminated. It appears that the PS chemical structure is a key parameter. Indeed, it has been shown that parameters such as overall charge and distribution, and lipophilicity control cellular uptake and subcellular distribution of a PS [2].

PDT requires 3 elements that are all important. The researchers in PDT should optimize these 3 parameters. Concerning oxygen, it is important to avoid hypoxia [3]. Concerning light, it is necessary to use appropriate wavelengths and dosimetry (fluence and irradiance). The photosensitizer should absorb at the excitation wavelength (determination of molar extinction coefficient), be slightly fluorescent (for detection, determination of fluorescent quantum yield), and present phototoxicity (determination of singlet oxygen quantum yield (or other reactive oxygen species, ROS) but the photosensitizer should also have adequate physico-chemical properties to penetrate cancer cells and be as selective as

possible. Lipophilicity is one of the parameters that is interesting to determine to estimate the behavior of the PS in vivo.

Physicochemical characterization (solubility, ionization, lipophilicity, permeability) of newly synthesized compounds and PS provides useful information for predicting pharmacokinetic parameters and biological effects. Hydrophilic substances in their pharmacokinetic properties are inferior to lipophilic ones. They have lower bioavailability, a high metabolic rate and rapid elimination [4-10].

Lipophilicity determines the transfer of compounds in a biological system. It can affect the formation of a complex between a compound and a receptor or bio-macromolecule at the site of action. Lipophilicity encodes a significant amount of structural information that can be used to better understand the behavior of a solute in a biological environment by studying correlations with many physicochemical, pharmacokinetic, and pharmacodynamic properties of a drug, including absorption, distribution, metabolism, and excretion, as well as toxicity. The optimal lipophilicity range of a compound is the main driving force, which effectively controls the kinetic and dynamic aspects of drug action.

The hydrophilic/lipophilic balance of PS is one of the factors that will influence its biological behavior, such as absorption by cancer cells, intracellular localization, biodistribution and pharmacokinetics [11]. Lipophilic PSs will tend to bind low density lipoprotein (LDL) bound and will be more likely to achieve LDL receptor-mediated endocytosis. Hydrophobic PSs have been engineered to increase their accumulation in tumors. To avoid biological aggregation, it is possible to use nanoparticles (liposomes, lipoproteins, micelles). Hydrophilic photosensitizers are more soluble in blood, but they do not penetrate with ease cancer cells and present very often fast clearance. Amphiphilic compounds, which

contain both hydrophilic and hydrophobic moieties in their molecular structure, are promising [12].

The distribution of a substance between water and octanol is one of the criteria for determining the lipophilicity of a compound. The distribution coefficient D is taken as a quantitative descriptor of lipophilicity and is most commonly used in logarithmic form, Log*D*. The partition coefficient between water and n-octanol is defined as the ratio of the equilibrium concentrations of the test substance in n-octanol saturated with water and water saturated with 1-octanol. The Log*P* solely applies to neutral compounds, whereas the partitioning of ionizable chemicals is characterized by the distribution coefficient (Log*D*), which considers both neutral and charged species.

Experimental procedures for measuring Log*D* are well established [13-15]. The lipophilicity of a compound is usually measured by its distribution in either a two-phase system, liquid-liquid (octanol-water system), or solid-liquid (retention in reversed-phase high-performance liquid chromatography (RP-HPLC)). Although experimentally determined values are preferred, computational approaches have some advantages, since they do not require expensive equipment or reagents and are less time-consuming than experimental work. Many calculation methods have been developed now, and almost all of them can be divided into two main groups: approaches based on substructures and properties [16-24].

In most cases, different calculation methods lead to a significant discrepancy in the log*P* values for the same molecule (by 2–3 orders of magnitude), which may limit the use of these methods on a large scale. However, in some cases a quantitative correction of the differences between experimentally determined and calculated lipophilicity parameters can be

achieved by introducing a correlation coefficient calculated between the retention factors obtained by two methods [25].

The substance distribution between the two phases is closely related to the electronic structure of the solvated molecules. Therefore, quantum chemistry methods can also be used in this type of research. Recently, it has become possible to accurately describe the state of the electronic structure of single molecules in a solvent medium [26].

This study presents the results of determining and comparing the lipophilicity of three selected PS protoporphyrin IX (PpIX), pyropheophorbide-a (PPa), and photofrin (PF), using octanol-water distribution methods (Shake-flask), reversed-phase HPLC and theoretical density functional theory (DFT) calculations. The amount of existing experimental data Log*D*, including for the studied group of compounds, is insignificant and insufficient. This article describes and compares the results of determining the lipophilicity of the studied group of compounds obtained by various methods.

2 | MATERIALS AND METHODS

2.1 | Spectrophotometer

UV-3600 (Shimadzu) UV-Vis double beam spectrophotometer was used to perform absorbance measurements in quartz cuvettes with an optical path length of 1 cm. The UV-Vis spectra of electromagnetic waves in the 330-730 nm range were registered.

2.2 | Buffer preparation

250 mL of 1-octanol was used to saturate 1 L of Milli-Q and left overnight at 25-27°C. After complete separation of the two immiscible solvents, the bottom layer was separated using a

separatory funnel. 4.18 g of 3-(N-morpholino)propanesulfonic acid (MOPS) powder was dispersed in 1 L water, saturated with 1-octanol and the pH was adjusted to 7.4 [27].

2.3 | Preparation of samples for injection

PpIX, PPa and PF stock solutions were prepared by weighing the exact amount of powders with a concentration of 1 $mgmL^{-1}$. 0.20 μm syringe filters were used to filter the stock solutions. PpIX and PF stock solutions were injected in HPLC directly after filtering whereas the final sample concentration of PPa was 50 μgmL^{-1}.

2.4 | HPLC conditions

HPLC experiments were conducted with a Varian setup equipped with 2 Prostar 210 pumps, a reversed-phase Varian Pursuit column (5 μm, 4.6 mm * 150 mm), a PDA UV-visible detector and a fluorescence detector. The Varian Star Chromatography system performed data acquisition. Different trials were carried out with an isocratic acetonitrile-buffer mobile phase, and 1 $mL \cdot min^{-1}$ flow rate was chosen to elute the samples during the whole experiment. 0.45 μm membrane filter was used to filter the mobile phase before the use. The different ratios of acetonitrile (with 0.25% 1-octanol) and buffer were used to elute the samples of PpIX, PF and PPa at 75:25, 80:20, 85:15 (v/v) ratios. UV detection was used at λ = 415 nm. 50 μL of sample or acetonitrile (blank) was injected for 20 min sample run time.

2.5 | Computational method

Gaussian 16 program package [28] was used to calculate the partition coefficient of PpIX and PPa. DFT method with two functionals: B3LYP (Becke's three parameter Lee–Yang–Parr) [29, 30], ωB97X-D [31] were set to optimize geometries of the studied molecules in *n*-octanol

and water. Within all calculations, the 6-31G(d), 6-31+G(d,p) and 6-311++G(d,p) basis sets were employed for both the B3LYP and ωB97X-D level of theory.

SMD, C-PCM and IEF-PCM implicit continuum models were chosen to approximate the influence of the solvents. The optimized structures were confirmed to be real minima by vibration analysis (no imaginary frequencies). The theoretical logarithm of the partition coefficient (DFT-log*P*) for the water/n-octanol mixture was calculated according to the following equation:

$$DFT - \log P = \frac{\Delta G_{water} - \Delta G_{n-octanol}}{2.303RT} \qquad (1)$$

where Δ*G* values are the Gibbs energies of the solvated molecules in the relevant solvent. For each PSs/method combination, the same methodology has been applied. The first step was to optimize the geometry in the gas phase. This geometry was used as a starting point for the second step of the geometry optimization, which was performed in the various implicit solvent models. Then, the logarithms of partition coefficients were evaluated based on the Gibbs energies from the optimized structure (Eq. 1). The distribution coefficient of two PSs was calculated by the following equation [32]:

$$LogD_{7.4} = \log P - \log(1+10^{(pH-pKa)}) \qquad (2)$$

where pH is the negative logarithm of the hydrogen ion activity, and pK_a is the negative logarithm of the dissociation constant (K_a) of the propionic acid group in PSs.

3 | RESULTS AND DISCUSSION

Three PSs have been chosen for this study. Our group already described the photophysical

properties of these compounds [33]. Their chemical structures are shown in figure 1. It is important to notice that amphiphilic properties of PpIX come from two propionate groups, which are grafted onto a hydrophobic ring core [34] since the propionic acid is a weak acid, it dissociates partly at physiological pH=7.4 with a pK_a value of 4.87. PPa is a porphin, with four pyrrole rings linked by methylene bridges with one propionate group [35]. PF is a mixture of hematoporphyrin oligomers purified from less active monomers [36].

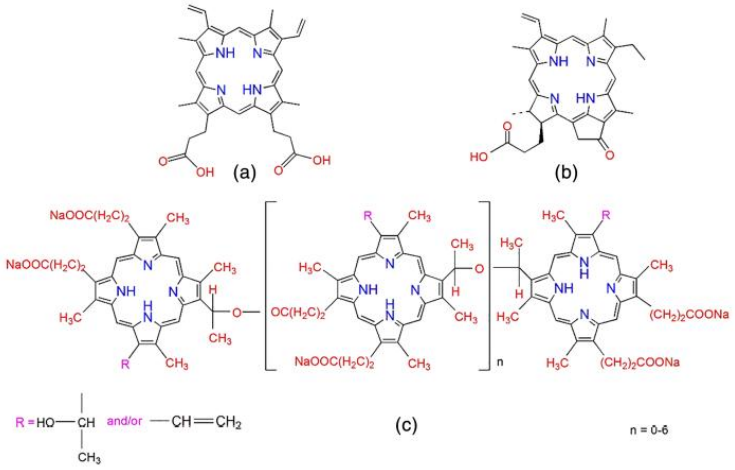

FIGURE 1 Molecular structures of PpIX (a), PPa (b), and PF (c)

3.1 | Measurement of lipophilicity by spectrophotometric method

The lipophilicity of the compounds was determined by the traditional shake-flask method in n-octanol/water Milli-Q at 37°C. 10 µL of 10 mM compounds in DMSO were mixed with n-octanol and water Milli-Q in a 50/50 ratio test tube. Test tubes were shaken at 37°C for 3 hours and then allowed to stand for 24 hours. After separation, 10 µL of each phase was taken and diluted in 3 mL of ethanol, and the absorbance of the solutions were measured by UV-vis. Log*D* values were calculated according to the following equation:

$$Log\,D = \log\left[\frac{A_{org}}{A_{aq}}\right] \quad (2)$$

where A_{org} and A_{aq} are the absorption of organic (n-octanol) and aqueous phase, respectively (Figure 2).

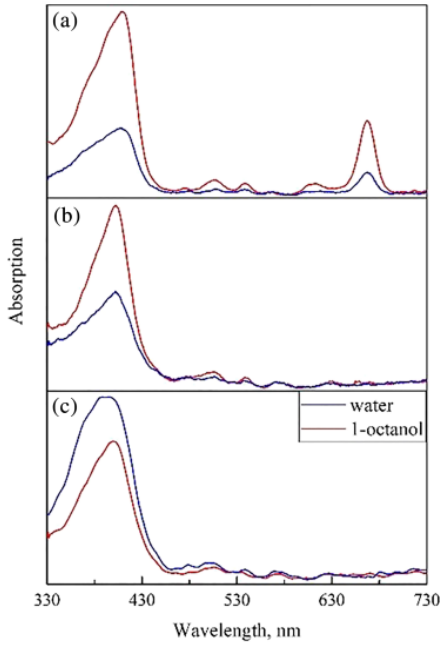

FIGURE 2 UV-vis absorption spectra of PPa (a), PpIX (b) and PF (c) in 1-octanol–water mixture

Table 1 summarizes the obtained Log*D* values (lipophilicity) which were defined and calculated as the logarithm of the ratio of the absorption of the compounds in the organic and aqueous phases.

The Log*D* of the PSs in the n-octanol-water system increases in a series of compounds PF<PpIX<PPa. A decrease in the number of polar carboxyl groups in the PPa lead to an increase in the Log*D* due to increased hydrophobicity of the molecule by stacking the porphyrin ring. The highest values of Log*D* are characteristic of PPa, which, in our opinion, is due to the lower ability of one carboxylic group to form hydrogen bonds with water molecules compared to PpIX and PF, which leads to a shift of two-phase equilibrium towards organic phase.

3.2 | Measurement of lipophilicity by HPLC

Retention time (t°) was measured by injecting acetonitrile along with the sample at three mobile ratios compared to the blank and repeated several times. To account for differences in HPLC, the capacity factor was used instead of the retention time [27]. The capacity factor (*K′*) is the retention time of a compound relative to a non-retentive chemical species (i.e., the solvent front):

$$K' = \frac{(t^R - t^0)}{t^0} \qquad (3)$$

Where, the capacitor factor of the solute at a certain concentration of the organic solvent is defined as *K′*, *t*° is the retention time of the non-retentive species, and t^R is the retention time of the sample. In this case, the time required for the empty solvent peak is used as t°. The logarithm of *K′* was extrapolated to a 0% acetonitrile concentration and plotted on the graph by plotting the logarithm of *K′* on the y-axis and the percent ratio of acetonitrile on

the x-axis [27]. The regression equation was created from the graph for each sample run and the log*D* of the test compound was calculated by log*K* at 0% acetonitrile (y-axis intercept). In the end, a comparison of the obtained experimental shake-flask and HPLC log*D* values was made.

HPLC was performed to determine the log*D* values of PSs. During the calculation of log*D* value concentration of the organic modifier was set at 0%, and a plot of the logarithm of the capacity factor (log*K*) against different concentrations of the organic solvent (acetonitrile) was done. Since isocratic elution was used as the method, retention times of the isocratic system were evaluated with different volume percentages of acetonitrile. Isocratic lipophilicity index was determined using the retention time and the capacity factor of the sample [27]. Before injecting the sample, the retention time of acetonitrile was determined (Fig.3). Subsequently, the test substances (1 $mgmL^{-1}$ PpIX, PF and 50 μgmL^{-1} PPa) were injected and eluted at the chosen ratios of the acetonitrile/buffer solution (see Fig. 4-6 for a demonstrative representation). Figs 3, 4 and 5 show the blank and sample retention time at 75, 80 and 85 % organic modifier, respectively. Figs 6-8 exhibit the overlay chromatogram of PpIX, PF, and PPa, showing the various retention times of acetonitrile and PS at different acetonitrile ratios.

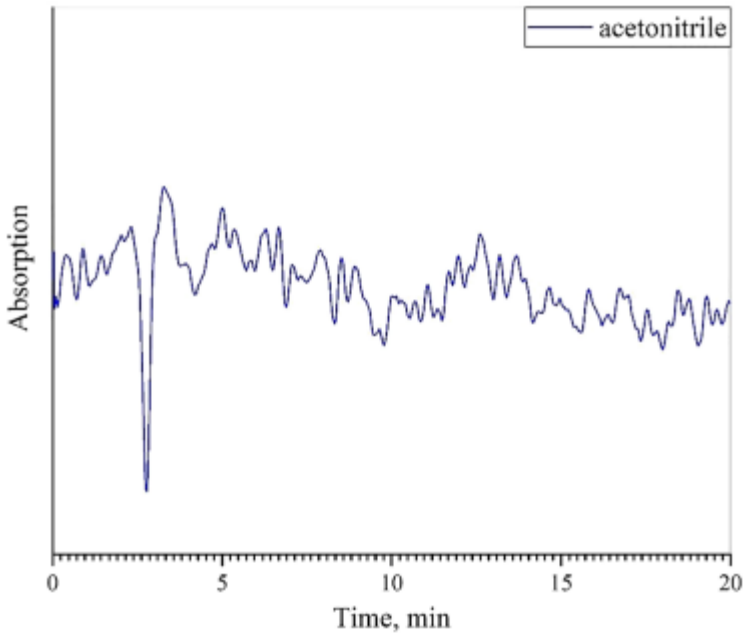

FIGURE 3 Retention time chromatogram of blank acetonitrile

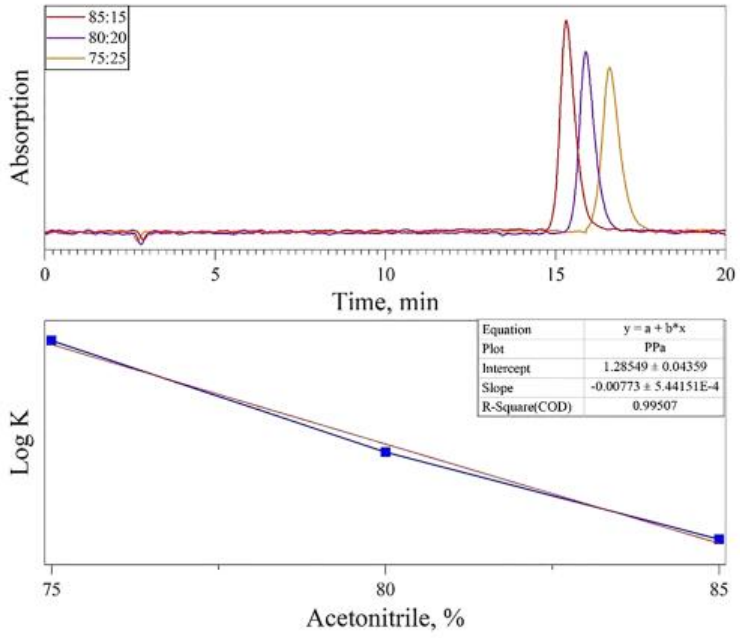

FIGURE 4 Retention time chromatogram (acetonitrile–buffer mobile phase) and plot (% acetonitrile vs log*K*') of PPa

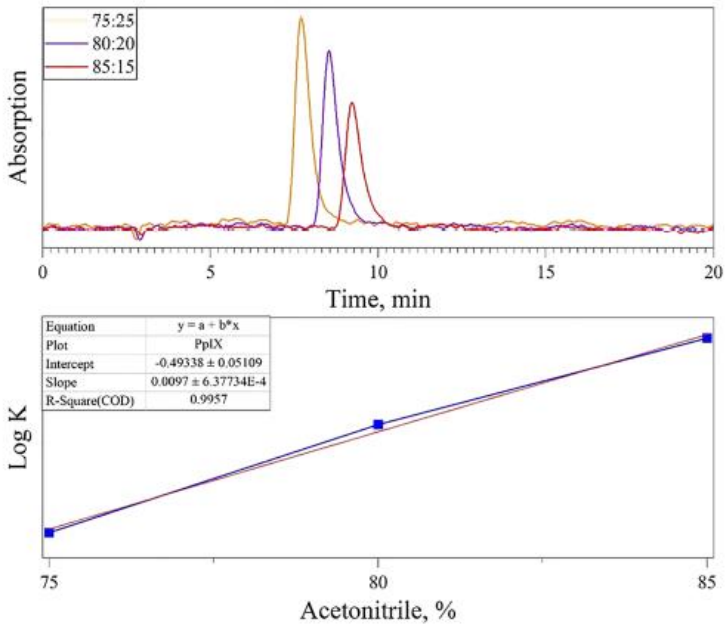

FIGURE 5 Retention time chromatogram (acetonitrile–buffer mobile phase) and plot (% acetonitrile vs log*K*') of PpIX

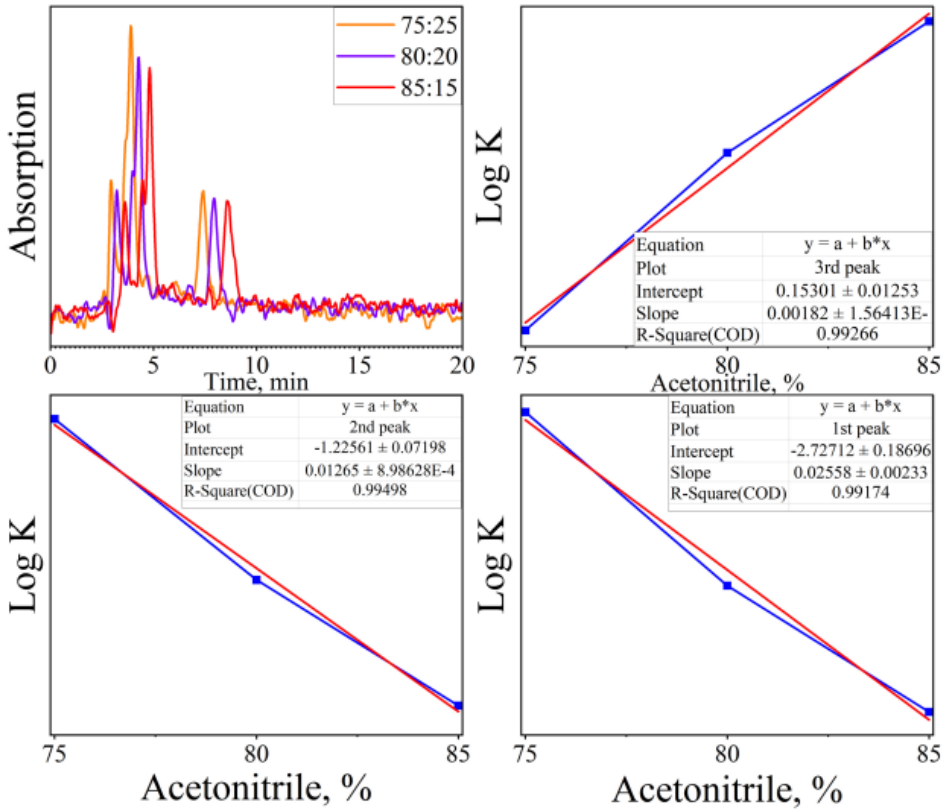

FIGURE 6 Retention time chromatogram (acetonitrile–buffer mobile phase) and plot (% acetonitrile vs log*K*') of PF

The results show that PpIX is more hydrophilic than PPa, with a value of -0.49 (1.29). This can be explained by the presence of the two propionic groups (Table 2). PF is amphiphilic, characterized by a complicated chemical structure with polar and apolar regions. In all cases, R^2-values of >0.99 were observed, indicating that the HPLC method is suitable for measuring the lipophilicity of PSs.

3.3 | Measurement of lipophilicity by DFT method

Literature values were determined by calculation since there is a lack of experimental works for porphyrin compounds. The Gaussian/DFT method was used only for small molecules until now because for compounds like porphyrins, the calculation is highly cost and needs longer operation time. That is why it was challenging for us to apply DFT method to large molecules. The different structures of PpIX have been obtained from conformational analysis at the B3LYP and WB97XD levels of theory (6-31G(d), 6-31+G(d,p) and 6-311++G(d,p) basis sets) using all solvent models in water and n-octanol. The lower energy conformer obtained at B3LYP/6-31+G(d,p), 6-311++G(d,p) level using SMD, C-PCM, IEF-PCM/water, and n-octanol shows two hydrogen bonds between the two carboxyl groups (Figure 7C, 7D, 7E and 7F). This probably results from a better description of long-range interaction such as hydrogen bonds with the WB97XD level of theory and 6-311++G(d,p) basis set. However, another low energy conformer of PpIX was observed at the B3LYP/6-31G(d) level in all solvent models (water and n-octanol) but also at the WB97XD/6-31G(d) level of theory in SMD/water (Figures 9). In this case, only one hydrogen bond is observed between the two carboxylic groups. In this latter conformation, the propionic acid group remained in the same plane as the porphyrin ring, while the other group was rotated. On the other hand, DFT calculation presents the same conformation of PPa at both B3LYP and WB97XD level of theories in all three basis

sets using SMD, C-PCM, IEF-PCM/water, and n-octanol systems (Figures 10-11). The computational methods have shown no effect on the conformation of PPa, which can be interpreted by the more rigid structure of PPa in contrast to PpIX.

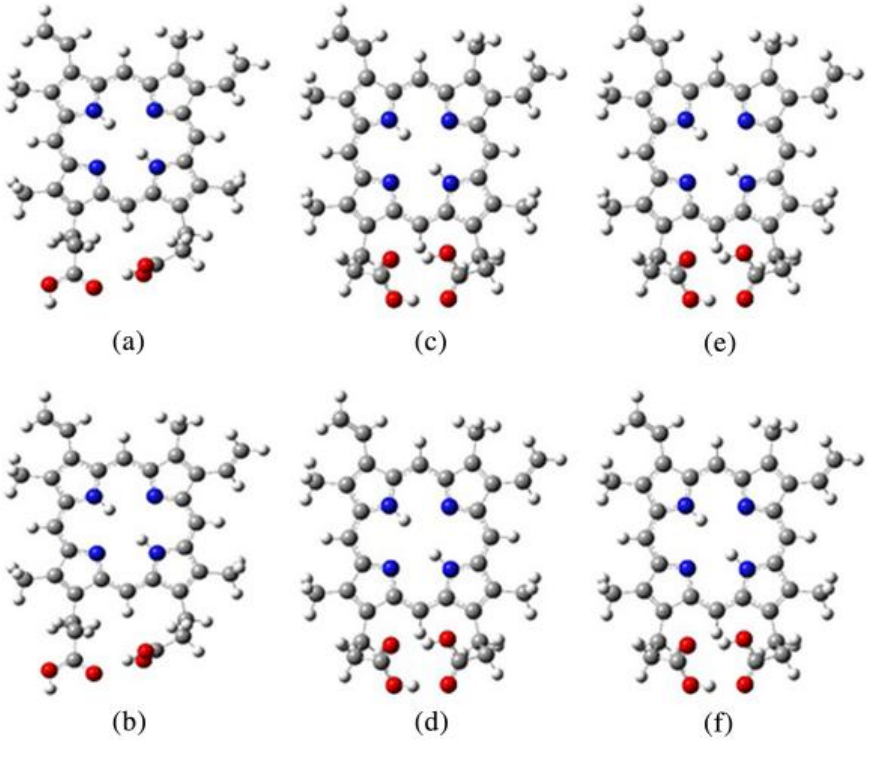

FIGURE 7 The optimized structure of PpIX in water (a, c, e), *n*-octanol (b, d, f) in B3LYP by 6-31G(d), 6-31+G(d,p) and 6-311++G(d,p) basis sets in all solvent models

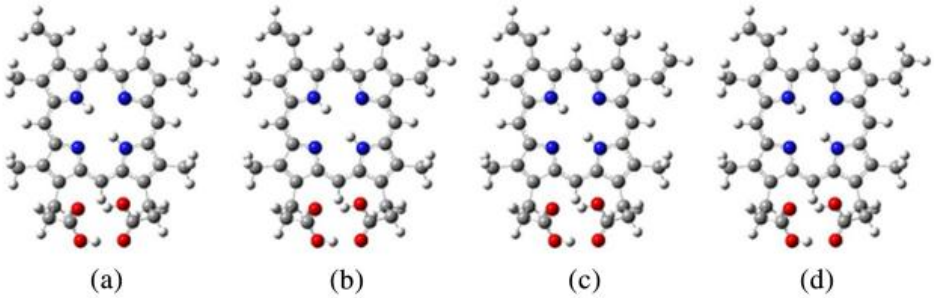

FIGURE 8 The optimized structure of PpIX in water (a, b), *n*-octanol (c, d) in WB97XD by 6-31+G(d,p) and 6-311++G(d,p) basis sets in all solvent models

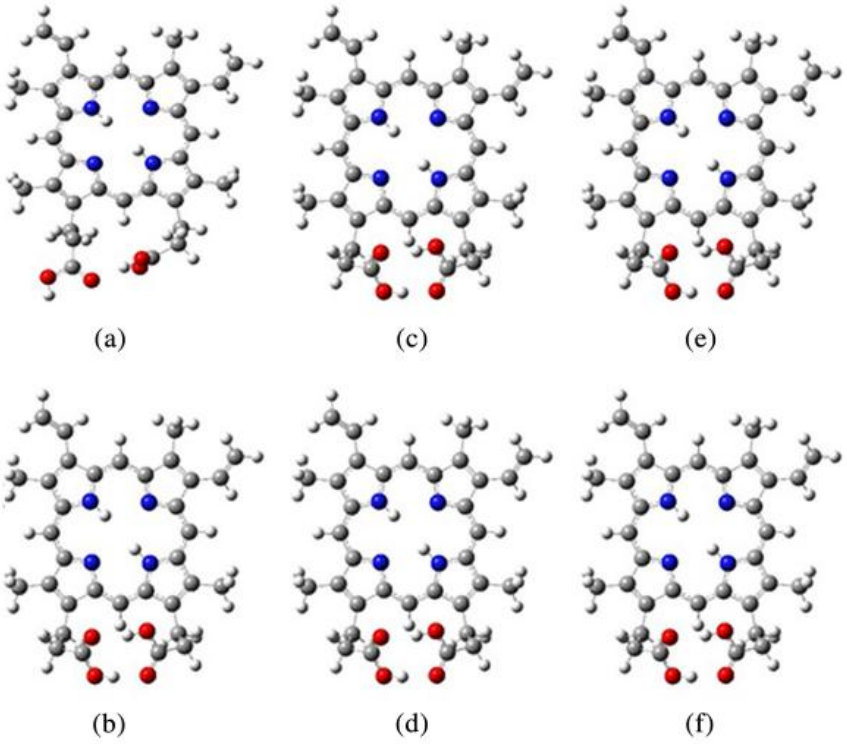

FIGURE 9 The optimized structure of PpIX in water (a, c, e), *n*-octanol (b, d, f) in WB97XD by 6-31G(d) basis set in SMD, C-PCM and IEF-PCM

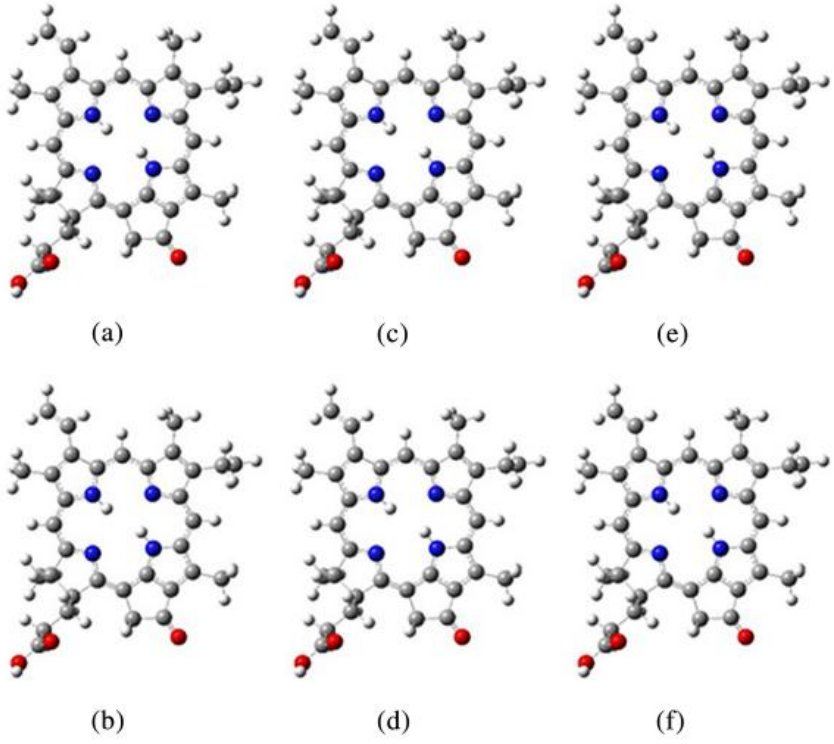

FIGURE 10 The optimized structure of PPa in water (a, c, e), *n*-octanol (b, d, f) in B3LYP by 6-31G (d), 6-31+G(d,p) and 6-311++G (d,p) basis sets in all solvent models

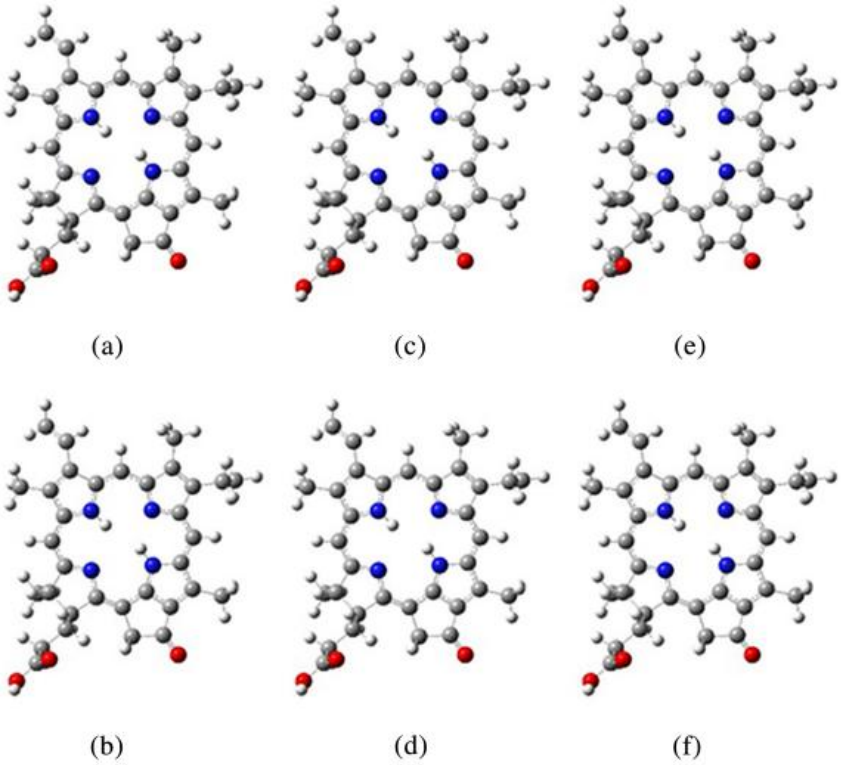

FIGURE 11 The optimized structure of PPa in water (a, c, e), *n*-octanol (b, d, f) in WB97XD by 6-31G(d), 6-31+G(d,p) and 6-311++G(d,p) basis sets in all solvent models

As can be seen from Table 3, the results of calculating the partition coefficient might have some discrepancies with the literature data. This may be due to the specified calculation conditions (pH and temperature), which depend on many factors and may change over time under the experimental conditions.

The obtained theoretical results are shown in Table 3. The positive cLog*P* value within the SMD model was obtained for PpIX and PPa by B3LYP and WB97XD functionals. All calculated cLog*P* values of PpIX and PPa were negative from –0.90 to –1.33 for C-PCM and from –1.34 to –1.91 for IEF-PCM implicit models. The B3LYP functional predicted the highest value of cLog*P* for both PSs though lower values were obtained within the WB97XD functional. The same tendency was observed when the basis set was changed from 6-31G(d) to 6-311++G(d,p). It can be seen that PPa (cLog*P*=3.39) is more hydrophobic than PpIX (cLog*P*=2.05), which was proved by UV-Vis and HPLC results.

Literature values were determined only by calculation (ALOGPS and CHEMAXON), and no experimental values could be found (Table 4). Indeed, determining LogP by ALOGPS and CHEMAXON method induces an overestimation. Moreover, PF is a mixture of molecules, and the results obtained by HPLC (3 different LogP) seem closer to reality. For PpIX, whatever method we used, we always got a lower value than the literature values. As we already mentioned, Gaussian/DFT method induces an overestimation. PpIX has two propionic acid groups and at pH=7.4, only one of them can be deprotonated. The low value we obtain by shake-flask or HPLC are in agreement with this (Table 5).

Log*D* values of PpIX obtained by Shake-flask and HPLC methods were close to DFT calculated values and the same results were observed for PPa. As it can be seen from table 5, the computed values of two basis sets with the WB97XD functional showed very close values to experimental results.

Additionally, as a result of these studies, it was found that there is a direct relationship between lipophilicity and fluorescence, and singlet oxygen quantum yields. That is, as can be seen from Table 6 [33], in a nonpolar solvent, the fluorescence quantum yield of PPA is the highest, but for PF it is the opposite. This means that as a result of lipophilicity, PF is well distributed in an aqueous environment and therefore presents high fluorescence quantum yield in polar solvents. Concerning PpIX, the lipophilicity is lower compared to PPa, but higher than PF. Accordingly, fluorescence quantum yield values are observed between the values of these two PSs. Regarding the singlet oxygen quantum yield, it was detected only for PF in aqueous media. Because PF is amphiphilic, which shows both polar and nonpolar properties from the lipophilicity results. Therefore, singlet oxygen quantum yield was calculated in both solvent.

4 | CONCLUSIONS

The lipophilic properties of drugs are essential, since hydrophilic properties facilitate the administration and delivery in the bloodstream and intercellular fluid to therapeutic targets, and the hydrophobic ones penetrate cells.

The experiment and calculation were performed to gain knowledge about the molecular behavior of PSs. The lipophilicity of PpIX, PPa, and PF was calculated theoretically and measured experimentally for the first time.

The Shake Flask Method was rather time-consuming, and the obtained Log*D* values of PSs followed the tendency of lipophilicity of the molecules which PPa is the most hydrophobic with values of 0.30-0.45.

HPLC was a faster technique that could be used with the known structure of the solute. This method is suggested to predict a compound's lipophilicity based on obtained chromatographs accurately. The results obtained by the HPLC method were in good correlation with the shake flask method. The Log*D* of PpIX was positive and negative by the shake-flask method and HPLC, respectively, but the values were close (0.24 and –0.49). Interestingly, there were observed three peaks and calculated three Log*D* values for PF which proved the amphiphilic nature of this PS. The calculated two values describe polar and one value shows apolar properties of PF (–2.73, –1.23, and 0.15 respectively).

Log*P* values can be predicted by different theoretical chemistry methods making it a powerful resource, which can be done without a compound sample. In other words, DFT with hybrid (B3LYP) and long-range (WB97XD) functional was highlighted as an important tool for the lipophilicity calculation of PSs. SMD, C-PCM and IEF-PCM implicit solvent models

were applied with 6-31G(d), 6-31+G(d,p) and 6-311++G(d,p) to estimate Log*P* values of PpIX and PPa. The structure complexity of PF did not make it to calculate Log*P* of this PS. It can be concluded that basis sets are the main parameters than functional to be controlled during the prediction of Log*P*.

Our HPLC and DFT calculations reveal that PPa is the most hydrophobic and can boost its accumulation in tumors and improve PDT results. The problem of hydrophobic PPa aggregation in biological fluids can be solved by using liposome, lipoprotein, or micelle-based delivery vehicles. The HPLC results found that PpIX will be easier to prepare for *in vivo* injection, but it is less likely to infiltrate cancer cells and clear the body more quickly. PF is versatile and promising for clinical translation because it contains both hydrophilic and hydrophobic components in their chemical structure. The choice of the ideal drug-to-light interval, as well as the ability to accomplish PF accumulation in both individual cell organelles and intracellular regions, is largely determined by its pharmacokinetics and biodistribution.

Experimental and computational data presented in this paper show the possibility of determining the partition coefficient of photosensitizers, which have high photodynamic activity in PDT. The obtained results on determining photosensitizers' lipophilicity may be useful in drug development in the field of PDT.

ACKNOWLEDGMENTS

This work has been supported in part by ERASMUS +. We would like to thank the program ERASMUS + (Mobility for study) for the financial support and the University of Lorraine for the use of Explor mesocentre.

REFERENCES

[1] A.P. Castano, P. Mroz and M.R. Hamblin, *Nat. Rev. Cancer*. **2006**, 6, 535–545.

[2] R.W. Boyle and D. Dolphin, *Photochem. Photobiol*. **1996**, 64, 469–485.

[3] L. Larue, B. Myrzakhmetov, A. Ben-Mihoub, A. Moussaron, N. Thomas, P. Arnoux, F. Baros, R. Vanderesse, S. Acherar and C. Frochot, *Pharmaceuticals*. **2019**, 12, 163.

[4] R. Mannhold, G.I. Poda, C. Ostermann and I.V. Tetko. *J. Pharm. Sci*. **2009**, 98, 861–893.

[5] F. Lombardo, E. Gifford and M.Y. Shalaeva. *Mini Rev. Med. Chem*. **2003**, 3, 861–875.

[6] B. Testa, B. Verlag Helvetica Chimica Acta and Willey-VCH, Zürich and Weinheim, Zwitzerland and Germany, **2006**.

[7] H. Van de Waterbeemd, H. Wiley-VCH, Weinheim, Germany, **2003**.

[8] F. Atkinson, S. Cole, C. Green and H. Van de Waterbeemd. *Cent. Nerv. Syst. Agents Med. Chem*. **2002**, 2, 229–240.

[9] M.T.D. Cronin. *Curr. Computer-Aided Drug Des*. **2006**, 2, 405–413.

[10] B. Testa, P. Crivori, M. Reist and P.A. Carrupt. *Perspect. Drug Discov. Des*. **2000**, 19, 179–211.

[11] R. Saavedra, L.B. Rocha, J.M. Dąbrowski and L.G. Arnaut. *ChemMedChem*. **2014**, 9, 390–398.

[12] E. Ö. Gündüz, M. E. Gedik, G. Günaydın and E. Okutan. *ChemMedChem*. **2021**, 17, e202100693.

[13] E. Rutkowska, K. Pajak and K. Jóźwiak. *Acta Pol. Pharm*. **2013**, 70, 3–18.

[14] G. Klopman and H. Zhu. *Mini Rev. Med. Chem*. **2005**, 5, 127–133.

[15] H. Zhu, A. Sedykh, S.K. Chakravarti and G. Klopman. *Curr. Computer-Aided Drug Des*. **2005**, 1, 3–9.

[16] A.Y. Sedykh and G. Klopman. *J. Chem. Inf. Model*. **2006**, 46,1598–1603.

[17] I.V. Tetko, J. Gasteiger, R. Todeschini, A. Mauri, D. Livingstone, P. Ertl, V.A. Palyulin, E.V. Radchenko, N.S. Zefirov, A.S Makarenko, V.Y. Tanchuk and V.V. Prokopenko. *J. Computer-Aided Mol. Des*. **2005**, 19, 453–463.

[18] E. Benfenati, G. Gini, N. Piclin, A. Roncaglioni and M.R. Vari. *Chemosphere*. **2003**, 53, 1155–1164.

[19] F. Vlahovići, S. Ivanović, M. Zlatar and M. Gruden. *J. Serb. Chem. Soc*. **2017**, 82, 1369–1378.

[20] D.J. Livingstone, M.G. Ford, J.J. Huuskonen and D.W. Salt. *J. Computer-Aided Mol. Des*. **2001**, 15, 741–752.

[21] Y. Zhao and D.G. Truhlar. *Theor. Chem. Account*. **2008**, 120, 215–241.

[22] J.A. Arnott and S.L. Planey. *Expert Opin. Drug Discov*. **2012**, 7, 863-875.

[23] S. Grimme, S.Ehrlich and L. Goerigk. *J. Comput. Chem*. **2011**, 32, 1456–1465.

[24] A.V. Marenich, C.J. Cramer and D.G. Truhlar. *J. Phys. Chem. B*. **2009**, 113, 6378–6396.

[25] M. Szeląg, D. Mikulski and M. Molski. *J. Mol. Model*. **2012**, 18, 2907–2916.

[26] M. Michalík and V. Lukeš. *Acta Chim. Slov*. **2016**, 9, 89–94.

[27] K. Venkata Sairam, B.M. Gurupadayya, B. Vishwanathan Iyer and R.S. Chandan. *Int. J. Pharm. Pharm. Sci*. **2017**, 9, 98–104.

[28] M. J. Frisch, G. W. Trucks, H. B. Schlegel, G. E. Scuseria, M. A. Robb, J. R. Cheeseman, G. Scalmani, V. Barone, G. A. Petersson, H. Nakatsuji, X. Li, M. Caricato, A. V. Marenich, J. Bloino, B. G. Janesko, R. Gomperts, B. Mennucci, H. P. Hratchian, J. V. Ortiz, A. F. Izmaylov, J. L. Sonnenberg, D. Williams-Young, F. Ding, F. Lipparini, F. Egidi, J. Goings, B. Peng, A. Petrone, T. Henderson, D. Ranasinghe, V. G. Zakrzewski, J. Gao, N. Rega, G. Zheng, W. Liang, M. Hada, M. Ehara, K. Toyota, R. Fukuda, J. Hasegawa, M. Ishida, T. Nakajima, Y. Honda, O. Kitao, H. Nakai, T. Vreven, K. Throssell, J. A. Montgomery, Jr., J. E. Peralta, F. Ogliaro, M. J. Bearpark, J. J. Heyd, E. N. Brothers, K. N. Kudin, V. N. Staroverov, T. A. Keith, R. Kobayashi, J. Normand, K. Raghavachari, A. P. Rendell, J. C. Burant, S. S. Iyengar, J. Tomasi, M. Cossi, J. M. Millam, M. Klene, C. Adamo, R. Cammi, J. W. Ochterski, R. L. Martin, K. Morokuma, O. Farkas, J. B. Foresman, and D. J. Fox, *Gaussian, Inc*. **2016**.

[29] A.D. Becke. *Phys. Rev. A,* **1988**, 38, 3098-3100.

[30] C. Lee, W.T. Yang and R.G. Parr. *Phys. Rev. B*, **1988**, 37, 785-789.

[31] J.D. Chai and M. Head-Gordon. J. Chem. Phys. **2008**, 128, 084106.

[32] T.D. Bergazin, N. Tielker, Y. Zhang, J. Mao, M.R. Gunner, K. Francisco, C. Ballatore, S.M. Kast and D.L. Mobley. *J. Comput. Aided Mol. Des*. **2021**, 35, 771–802.

[33] B. Myrzakhmetov, P. Arnoux, S. Mordon, S. Acherar, I. Tsoy and C. Frochot. *Pharmaceuticals*. **2021**, 14, 138.

[34] L.M. Scolaro, M. Castriciano, A. Romeo, S. Patanè, A. Cefalì and M.G. Allegrini. *J. Phys. Chem. B*. **2002**, 106, 2453–2459.

[35] L. Delanaye, M. Bahri, F. Tfibel, M. Fontaine-Aupart, A. Mouithys-Mickalad, B. Heine, J. Piette and M. Hoebeke. *Photochem. Photobiol*. Sci. **2006**, 5, 317–325.

[36] A.T.P.C. Gomes, M.G.P.M.S. Neves and J.A.S. Cavaleiro. *An Acad. Bras. Cienc*. **2018**, 90, 993–1026.

[37] https://go.drugbank.com/drugs/DB02285.

TABLE 1 Absorption wavelength (nm) and determination of log*D* with the traditional shake-flask method in n-octanol/water Milli-Q at 37°C (shaking 3 hours, measurement 24 hours after)

Compound	**Wavelength, nm**	**Log*D*** **24 h**
Pyropheophorbide a (PPa)	409	0.45
Protoporphyrin ix (PpIX)	402	0.24
Photofrin (PF)	400	- 0.18

TABLE 2 Capacitor factor and obtained Log*D* results of PPa, PpIX and PF by HPLC method (UV detection at λ = 415 nm and 20 min sample run time)

PSs	ACN:buffer ratio	R_t of PSs	R_t of blank	*K*	Log*K*	Regression equation	R^2	Log*D*
PPa	75:25	16.58	2.72	5.095588	0.707194	y=-0.0077x+1.2855	0.9951	1.29
	80:20	15.88	2.83	4.611307	0.663824			
	85:15	15.32	2.91	4.264605	0.629879			
PpIX	75:25	7.80	2.88	1.708333	0.232573	y=0.0097x-0.4934	0.9957	-0.49
	80:20	8.54	2.91	1.934708	0.286615			
	85:15	9.22	2.94	2.136054	0.329612			
PF (1^{st} peak)	75:25	2.94	2.55	0.152941	-0.815480	y=0.0256x-2.7271	0.9917	-2.73
	80:20	3.22	2.65	0.215094	-0.667370			
	85:15	3.61	2.83	0.275618	-0.559690			
PF (2^{nd} peak)	75:25	3.89	2.55	0.525490	-0.279440	y=0.0127x-1.2256	0.9950	-1.23
	80:20	4.29	2.65	0.618868	-0.208400			
	85:15	4.82	2.83	0.703180	-0.152930			
PF (3^{rd} peak)	75:25	7.51	2.55	1.945098	0.288941	y=0.0018x+0.153	0.9927	0.15
	80:20	7.93	2.65	1.992453	0.299388			
	85:15	8.57	2.83	2.028269	0.307125			

TABLE 3 Calculated cLog*P* values of PpIX and PPa at B3LYP/ WB97XD/6-31G(d)/ 6-31G(d)/6-311++G(d,p)/SMD/C-PCM/IEF-PCM level of theory

B3LYP									
Basis set		6-31G(d)			6-31+G(d,p)			6-311++G(d,p)	
Solvent model		SMD	C-PCM	IEF-PCM	SMD	C-PCM	IEF-PCM	SMD	C-PCM	IEF-PCM
PSs	PpIX	4.50	-0.99	-1.46	4.43	-1.04	-1.66	3.69	-1.17	-1.79
	PPa	4.63	-0.90	-1.34	4.62	-0.91	-1.40	3.72	-0.92	-1.59
WB97XD									
Basis set		6-31G(d)			6-31+G(d,p)			6-311++G(d,p)	
Solvent model		SMD	C-PCM	IEF-PCM	SMD	C-PCM	IEF-PCM	SMD	C-PCM	IEF-PCM
PSs	PpIX	4.39	-0.96	-1.58	2.90	-1.07	-1.64	2.05	-1.11	-1.70
	PPa	4.32	-1.09	-1.64	3.88	-1.33	-2.12	3.39	-1.27	-1.91

TABLE 4 Log*P* values determined by DFT method and literature values computed by ALOGPS and CHEMAXON

cLog*P*		PpIX	PPa
B3LYP	6-31+G(d,p)	4.43	4.63
	6-31++G(d,p)	3.69	3.72
WB97XD	6-31+G(d,p)	2.90	3.88
	6-31++G(d,p)	2.05	3.39
Literature values		4.40 (37) 6.78 (37)	6.37 [37] [2-(1-Hexyloxyethyl)-2-devinyl pyropheophorbide-a] 7.53 [37] [2-(1-Hexyloxyethyl)-2-devinyl pyropheophorbide-a]

TABLE 5 Log*D* values obtained experimentally and calculated by DFT method

PSs	Log*D*		cLog*D*			
			B3LYP		WB97XD	
	Shake-flask	HPLC	6-31+G(d,p)	6-31++G(d,p)	6-31+G(d,p)	6-31++G(d,p)
PF	-0.18	-2.73 -1.23 0.15	-	-	-	-
PpIX	0.24	-0.49	1.9	1.16	0.39	-0.43
PPa	0.45	1.29	2.10	1.19	1.35	0.86

TABLE 6 Φ_f of PpIX, PPa and PF in different solvents and Φ_Δ in D_2O at room temperature (C = 1.87 μM).

Solvent	**ET (30)**	**Φ_f (± 0.01)**		
		PpIX	**PPa**	**PF**
Toluene	33.9	0.09	0.39	<0.01
AcOEt	38.1	0.06	0.34	<0.01
EtOH	51.9	0.08	0.39	0.07
MeOH	55.4	0.07	0.31	0.05
Glycerol	57.0	0.04	0.20	0.02
Water	63.1	<0.01	<0.01	0.01
PBS	≈ 63.1	<0.02	<0.01	0.01
SVF	-	<0.01	<0.01	<0.01
			Φ_Δ (± 0.01)	
D_2O	≈ 63.1	-		0.15